POLITECNICO DI TORINO

Master's Degree in Biomedical Engineering

Analysis of the effect of the respiration on features extracted from the electrocardiogram and the heart sounds

Supervisors
Prof. Ing. Marco Knaflitz
Ing. Noemi Giordano

Candidate
Alice Lolli

Academic Year 2024/2025

Contents

Bibliography 35

List of Abbreviations

AHF Acute Heart Failure

AM Amplitude Modulation

BNP B-type Natriuretic Peptides

BSS Blind Source Separation

BW Baseline Wander

CHF Chronic Heart Failure

CNN Convolutional Neural Network

CTI Cardiac Time Interval

CVD Cardiovascular Disease

DC Direct Current

DL Deep Learning

DWT Discrete Wavelet Transform

ECG Electrocardiogram

EDR ECG-Derived Respiration

EE Energy Expenditure

LVEF Left Ventricular Ejection Fraction

EMD ElectroMechanical Delay

FM Frequency Modulation

HF Heart Failure

HFimpEF Heart Failure with improved Ejection Fraction

HFpEF Heart Failure with preserved Ejection Fraction

HFrEF Heart Failure reduced Ejection Fraction

HFmrEF Heart Failure with midly reduced Ejection Fraction

HR Heart Rate

HVD Hilbert Vibration Decomposition

ICA Independent Component Analysis

LVET Left Ventricular Ejection Time

MIMU Miniaturized Magneto-Inertial Measurement Unit

ML Machine Learning

MR-proANP Mid-Regional Atrial Natriuretic Peptide

NT-proBNP N-terminal fragment of pro-BNP

PCA Principal Component Analysis

PCG Phonocardiogram

PCHIP Piecewise Cubic Hermite Interpolation

PDR PCG-Derived Respiration

PEP Pre-Ejection Period

PPG Photoplethysmogram

PZT Lead Zirconate Titanate

PWPT Perceptual Wavelet Packet Transform

QRS QRS Complex

RNN Recurrent Neural Network

RSA Respiratory Sinus Arrhythmia

SCG Seismocardiogram

SNR Signal-to-Noise Ratio

SPWVD Smoothed Pseudo-Wigner-Ville Distribution

STFT Short-Time Fourier Transform

S1 First heart sound

S2 Second heart sound

TST Total Systolic Time

WPT Wavelet Packet Transform

WVD Wigner-Ville Distribution

List of Figures

List of Tables

Chapter 1

Introduction

1.1 Clinical motivation: Acute Heart Failure Prevention and Home Monitoring

Cardiovascular diseases (CVDs) represent one of the leading causes of mortality worldwide, contributing substantially to the global burden of disease and imposing a significant strain on healthcare systems in terms of both clinical management and economic costs [1].This is also confirmed by a recent report from the World Health Organization, which highlights the continuous rise in the prevalence of cardiovascular diseases, representing a serious threat to public health. These conditions are often referred to as "silent killers" because, in their early stages, they present with mild or barely recognizable symptoms [2]. Among cardiovascular diseases, heart failure (HF) stands out as one of the most severe and complex to manage, as it is associated with high mortality, frequent hospitalizations, and a significant deterioration in quality of life. Despite the considerable scientific and technological advances achieved in recent years, HF-related mortality has shown a steadily increasing trend since 2011. This evidence underscores the need to adopt an approach that goes beyond the development of pharmacological therapies or life-saving devices, integrating long-term prevention strategies. Such an orientation enables not only more effective disease management but also the possibility of counteracting its onset and progression. In this context, it is essential to promote the advancement of digital technologies and wearable systems capable of ensuring continuous and non-invasive remote monitoring of cardiorespiratory dynamics, thereby supporting a more personalized and proactive model of care [3].

1.1.1 Overview of Heart Failure

It is important to provide a general overview of heart failure (HF), which is recognized as a complex and progressive clinical syndrome characterized by the heart's inability to deliver an adequate cardiac output in relation to the metabolic demands of the body. HF is a clinical syndrome and not a single pathological diagnosis, characterized by key symptoms such as breathlessness, fatigue, and swelling of the lower limbs. These latter may be accompanied by objective signs, including elevated jugular venous pressure, pulmonary crackles, and peripheral oedema [4]. HF is a condition that evolves over time and, for this reason, progresses through distinct clinical stages, described by the classification system from stage A to stage D, which outlines the continuous progression of the disease from initial risk conditions to the most advanced forms. A key clinical objective is the prevention of transition between the early stages, particularly the shift from an "at-risk" condition to "pre-HF." Advances achieved over recent decades in diagnostic techniques, pharmacological

therapies, and device-based interventions have led to a change in the demographic profile of patients with HF, who now include individuals with a higher average age. However, this evolution has made clinical management more complex due to the increased frailty of the affected population and the likely presence of multiple comorbidities. The most recent and internationally shared definition describes HF as a syndrome characterized by the presence of symptoms that develop in the context of structural or functional cardiac abnormalities, accompanied by objective evidence of systemic or cardiopulmonary congestion. It derives from a structural and/or functional abnormality of the heart, which consequently leads to increased intracardiac pressures and/or inadequate cardiac output, occurring both at rest and during physical activity [4]. From a clinical perspective, HF is further classified according to left ventricular ejection fraction (LVEF), distinguishing between heart failure with reduced ejection fraction (HFrEF, EF $< 40\%$), mildly reduced ejection fraction (HFmrEF, 41–49%), preserved ejection fraction (HFpEF, $\geq 50\%$), and improved ejection fraction (HFimpEF). systolic function. This categorization allows for differentiation of pathophysiological mechanisms and facilitates the tailoring of therapeutic strategies. At the basis of cardiac dysfunction, it is essential to identify the etiology to formulate an accurate diagnosis, as the underlying pathology determines the most appropriate therapeutic approach [3]. From an epidemiological perspective, HF represents one of the main cardiovascular syndromes, particularly in developed countries, with a prevalence estimated at around 1–2% of the adult population and an incidence of approximately 3–5 new cases per 1000 people per year. Despite improvements in the prevention and management of cardiovascular diseases, population aging has led to an overall increase in the number of cases. Prevalence indeed rises with age, increasing from approximately 1% in individuals under 55 years of age to over 10% in those aged 70 years or older. HFrEF and HFpEF forms appear to be comparable in terms of frequency, although European outpatient registries have reported a higher prevalence of HFrEF. More than half of affected patients are female, confirming the progressive demographic shift associated with this syndrome. Usually, in the majority of cases, HF is due to myocardial dysfunction, either systolic, diastolic, or both. Nevertheless, the development of the syndrome may also be influenced by valvular, pericardial, or endocardial disease, as well as rhythm and conduction disorders [4]. Various clinical conditions are recognized as risk factors associated with the development of heart failure (HF), including hypertension, type 2 diabetes mellitus, ischemic heart disease, obesity, and chronic kidney disease. In particular, hypertension represents one of the most significant causes, as the chronic increase in afterload induces progressive ventricular remodeling and impairment of diastolic function, thereby promoting the evolution toward heart failure [3]. Acute heart failure (AHF) may present as the first clinical episode of the syndrome or, more commonly, as an exacerbation of a previously known chronic condition. Patients with an acute onset tend to have higher in-hospital mortality, but overall show a more favorable post-discharge prognosis, with lower rates of mortality and rehospitalization compared to those with acute decompensation of chronic heart failure (CHF) [5–8]. AHF is defined as the rapid or progressive onset of symptoms and signs related to HF, of such severity as to require urgent medical intervention, often associated with an unplanned hospital admission.It also represents one of the leading causes of hospitalization in individuals over the age of 65. This is one of the reasons why it is associated with high mortality and recurrent hospital admissions, thereby contributing significantly to the overall healthcare burden of heart failure. The severity of the clinical condition depends on multiple factors, including the interaction between precipitating elements, structural cardiac abnormalities, and concomitant comorbidities, all of which contribute to shaping both in-hospital evolution and long-term prognosis [4].

1.1.2 Diagnosis and Treatment Approaches

Echocardiography is recognized as the primary diagnostic tool for the morpho-functional assessment of the heart. For diagnostic confirmation and risk stratification, the measurement of B-type natriuretic peptides (BNP), such as the N-terminal fragment of pro-BNP (NT-proBNP) or the mid-regional atrial natriuretic peptide (MR-proANP), provides essential support, particularly in acute forms. The treatment of AHF primarily aims to restore haemodynamic stability, relieve congestion, and correct hypoxaemia. During the acute phase, supportive interventions are employed, such as oxygen therapy in cases of hypoxia and intravenous administration of diuretics to reduce volume overload. In patients with adequate blood pressure, vasodilators may be used to improve symptoms, while the use of inotropic agents or vasopressors is reserved for more severe forms, characterized by hypoperfusion or cardiogenic shock. These treatments serve symptomatic and stabilizing purposes without directly affecting the long-term progression of the disease, and represent a necessary step to enable the optimization of chronic therapy once compensation is achieved [4].

1.1.3 Clinical needs and motivation for Home Monitoring

Despite advances in diagnosis and clinical management, the follow-up of patients with HF remains complex, particularly after episodes of acute decompensation, when the risk of rehospitalization is high. One of the main challenges lies in the difficulty of promptly detecting signs of deterioration, which often emerge gradually and in a subclinical manner. Traditional monitoring models, based on periodic check-ups, do not allow for continuous assessment of the patient's physiological status, limiting the possibility of early intervention. In recent years, the evolution of wearable technologies and remote monitoring systems has opened new perspectives both for screening in the general population and for remote surveillance of patients with HF. These devices enable continuous recording of physiological parameters, such as heart rate (HR) and rhythm, respiratory rate, physical activity, posture, blood pressure, weight, sleep, and blood glucose, which may provide useful indications for the early identification of clinical changes potentially associated with decompensation episodes. Clinical studies, such as the LINK-HF trial, have demonstrated the potential of a multisensor chest patch connected via telemetry to a smartphone, which processes the data through an artificial intelligence algorithm with the aim of predicting exacerbation events several days before actual hospitalization. This approach allows for early detection of clinical deterioration, offering the opportunity to intervene before hospitalization becomes necessary [9]. However, large-scale adoption of such tools remains limited by several factors, including signal noise, inter- and intra-patient variability, the need for robust algorithms to extract clinically relevant information, and the management of large volumes of data. Beyond technical challenges, operational issues persist, such as device cost, usability, patient engagement and adherence, and the complexity of data processing and interpretation. It is therefore essential to develop monitoring systems that are simple, reliable, and non-invasive, capable of ensuring accurate and stable collection of physiological signals over time and adaptable to a broad user population. Such solutions could significantly contribute to reducing the burden of hospitalizations by improving diagnostic timeliness and continuity of care in the management of heart failure.

1.2 Cardiac Time Intervals as Non-Invasive Markers of Cardiac Function

Cardiac Time Intervals (CTIs) represent a temporal measure of the sequence of mechanical events occurring during the cardiac cycle and serve as a key indicator of systolic function

and electromechanical synchronization of the heart. Among the main intervals considered are the Pre-Ejection Period (PEP), the Left Ventricular Ejection Time (LVET), the Total Systolic Time (TST), and the Electromechanical Delay (EMD). Their estimation enables a non-invasive description of myocardial contractile activity and the temporal coordination between electrical stimulus and mechanical response [10]. Alterations in CTIs have been correlated with various pathological conditions, including mitral valve stenosis, coronary artery disease [11, 12], arterial hypertension [13], atrial fibrillation, hypovolemia, and fluid responsiveness [14], chronic myocardial disease [12], as well as in the assessment of left ventricular systolic function [11,12]. This correlation makes them clinically valuable parameters for evaluating hemodynamic status and for longitudinal monitoring of ventricular function.

Table 1.1. Main CTIs and their physio-clinical significance.

Interval	**Definition**	**Physio-clinical significance**
PEP	Time between the onset of ventricular depolarization and the opening of the aortic valve	Reflects myocardial contractility and afterload; its prolongation indicates reduced systolic function or increased peripheral resistance
LVET	Interval between the opening and closing of the aortic valve	Represents the duration of ventricular ejection; a reduction is associated with impaired systolic function or elevated afterload
TST	Time between the onset of ventricular depolarization and the closure of the aortic valve	Provides an overall measure of mechanical systole duration
EMD	Interval between ventricular electrical activation and the closure of the mitral valve	Indicates the coordination between electrical and mechanical activity; alterations may reflect ventricular asynchrony or contractile dysfunction

In clinical practice, the opening and closing of cardiac valves are traditionally evaluated using echocardiographic techniques such as M-mode, Doppler, or Tissue Doppler Imaging. However, these methods require skilled operators and are not suitable for continuous monitoring. For this reason, recent years have seen growing interest in non-invasive and portable techniques for estimating CTIs, based on mechanical and acoustic signals from the chest, such as seismocardiogram (SCG) and phonocardiogram (PCG). Another promising approach involves the combined use of electrocardiogram (ECG) and PCG, which enables direct correlation between the heart's electrical activity and the mechanical events of valve opening and closure, offering a more comprehensive estimation of cardiac function. A recent study introduced a wearable system that integrates ECG electrodes and contact-based lead zirconate titanate (PZT) sensors for the simultaneous acquisition of electrical and acoustic cardiac signals. The device demonstrated high operational stability, with signal-to-noise ratios (SNR) of 44.13 dB for ECG and 30.04 dB for PCG, allowing reliable extraction of functional parameters such as PEP, LVET, and EMD. A comparative analysis conducted on healthy subjects and patients with coronary artery disease revealed significant differences in CTI values, highlighting the clinical potential of this approach for early diagnosis and non-invasive monitoring of cardiovascular conditions [2]. Further developments have expanded

this paradigm by introducing multimodal devices capable of simultaneously acquiring ECG, PCG, and extracting respiratory signals. In particular, one study demonstrated the feasibility of reliably estimating key CTIs (PEP and LVET) and respiratory parameters using a wearable patch, validating its accuracy against clinical-grade reference instruments. The integration of respiratory extraction techniques from both ECG and PCG signals confirmed consistency with reference measurements, underscoring the potential of multimodal analysis for joint assessment of cardiac and respiratory dynamics [15]. Overall, these findings support the growing relevance of CTIs as non-invasive markers of cardiac function and emphasize the importance of multimodal ECG–PCG respiration integration to enhance diagnostic precision and continuous monitoring capabilities—topics that will be further explored in the following sections dedicated to cardiorespiratory interaction and experimental signal analysis.

1.3 Respiratory Influence on Cardiovascular Signals

Spontaneous breathing induces cyclic variations in pleural, alveolar, transmural, and intra-abdominal pressures [16], which generate oscillations in venous return, ventricular preload, and afterload. These changes affect the cardiovascular system, producing a phenomenon known as cardiorespiratory coupling [17]. Several physiological mechanisms mediate this interaction: (1) the activation of pulmonary stretch receptors, which are stimulated during inspiration and trigger the Hering–Breuer reflex, inhibiting cardiac vagal motoneurons in the nucleus ambiguus and producing a positive chronotropic effect [17, 18]; (2) the pressure oscillations induced by the thoraco-abdominal pump, which modulate venous return and left ventricular afterload, generating cyclic variations in arterial pressure and activating the baroreflex, associated with a negative chronotropic response during expiration [18–20]; (3) the direct interaction between respiratory circuits in the brainstem and cardiac vagal preganglionic neurons, which contributes to the synchronization between respiratory activity and HR. The overall result of these mechanisms is the respiratory sinus arrhythmia (RSA), which consists of a rhythmic variation of HR synchronized with breathing, characterized by a shortening of the RR interval during inspiration and its prolongation during expiration [21]. RSA represents one of the main forms of cardiorespiratory interaction, together with cardioventilatory coupling, defined by the synchronization between the heartbeat and the onset of inspiration, and respiratory stroke volume synchronization, characterized by the synchronized variation of right and left ventricular stroke volumes over the respiratory cycle [22]. A recent study proposed a multimodal approach for estimating respiration from ECG and PCG signals, introducing the methods of ECG-derived respiration (EDR) and PCG-derived respiration (PDR). From the ECG signal, respiration is obtained through variations in HR, amplitude, and morphology of the QRS complex (QRS), whereas from the PCG signal it is estimated based on the amplitude, area, and shape oscillations of the first heart sound (S1) and the second heart sound (S2), which are themselves modulated by the respiratory cycle. The PEP is instead derived by combining ECG and PCG, since it depends on both the electrical and mechanical domains. n total, twelve beat-to-beat features were extracted, belonging to four main classes: timing (HR, PEP, LVET), area (QRS_{area}, $S1_{\text{area}}$, $S2_{\text{area}}$), amplitude (QRS_{amp}, $S1_{\text{amp}}$, $S2_{\text{amp}}$), and morphology, obtained through principal component analysis (PCA), (QRS_{PCA}, $S1_{\text{PCA}}$, $S2_{\text{PCA}}$) [15]. These quantities, influenced by respiratory dynamics, were interpolated and filtered to obtain continuous respiratory signals and subsequently used in a regression model with cross-validation to estimate the respiratory flow and respiratory rate. The results showed a strong correlation between the derived and reference signals, confirming that respiration significantly modulates the temporal, morphological, and amplitude components of cardiovascular signals, thereby providing

a quantitative basis for the analysis of cardiorespiratory interactions.

1.4 Research Hypothesis and Objectives

1.5 Structure of the Thesis

Chapter 2

State of the Art

2.1 ECG and PCG in Cardiac Monitoring

ECG and PCG signals are widely recognized as key physiological markers of cardiac function, each providing complementary perspectives on the heart's activity [23]. The former provides information on the electrical activity of the heart, whereas the latter captures the mechanical vibrations generated by cardiac structures, particularly during valve closure [24, 25]. The auscultation of heart sounds is a commonly employed clinical practice aimed at rapidly assessing the condition of the cardiovascular system. The main sounds, S1 and S2, are associated with the closure of the heart valves and represent a fundamental reference for the analysis of cardiac function. However, in real-world conditions, the distinction of heart sounds is often challenging. Interpretation is influenced by interindividual variability, related to variations in training and experience among clinicians, as well as intraindividual variability, which reflects signal changes due to the presence of murmurs and additional heart sounds. During measurement, the ECG signal is frequently integrated with the PCG, as this combination allows the correlation of electrical and mechanical events of the cardiac cycle. This enables a more precise identification of the systolic and diastolic phases, improving the reliability of S1 and S2 recognition [26]. The information extracted from the joint analysis of ECG and PCG signals provides a robust foundation for the early identification of cardiovascular anomalies [27]. By leveraging the temporal alignment and complementary nature of these biosignals, clinicians can detect subtle deviations that may escape traditional single-modality assessments, thereby enhancing diagnostic precision and enabling timely intervention. Technological progress has underscored the limitations of traditional diagnostic methods based on heart sound auscultation, leading to the need for advanced solutions. Among these, the development of digital, portable, and wearable devices capable of concurrently acquiring both biosignals has emerged as crucial step forward [2]. It thus becomes possible to extract features derived both from the integrated and individual analysis of the two signals, such as PEP and LVET, which provide important temporal information for identifying cardiovascular dysfunctions [15].

2.2 Detection of Heart Sounds and Estimation of CTIs

The main heart sounds, S1 and S2, are generated by mechanical vibrations produced by the cardiovascular system [28–31]. These vibrations primarily result from the closure of the heart valves, events driven by pressure variations between the different cardiac chambers, but may also reflect myocardial wall contraction and blood flow turbulence within the great vessels [32]. The origin of S1 and S2 derives from the combination of multiple

valvular components. The first sound is produced by the closure of the atrioventricular valves, mitral and tricuspid, occurring at the onset of ventricular systole when the intraventricular pressure exceeds the atrial pressure. The second sound consists of aortic and pulmonary components, corresponding to the asynchronous closure of the semilunar valves. This event takes place at the onset of diastole, when ventricular pressure drops below that of the aorta and pulmonary artery [33]. Given the composite nature of heart sounds and the variability introduced by both physiological and pathological conditions, detection methods capable of accurately identifying S1 and S2 within cardiac biosignals are essential. It is therefore useful to provide an overview of the models proposed in the literature for heart sound detection. According to the study by Amit et al. [34], computational techniques such as clustering and classification have been used to identify the morphological variations induced by respiratory activity. The work presented in [35] demonstrated that the timing of the first heart sound varies systematically with respiration, increasing during inspiration and decreasing during expiration. However, this relationship is not linear and was modeled in Tang et al. (2015) [32] using Hammerstein-Wiener approach, enabling quantitative analysis for hemodynamic monitoring. For the analysis of the second heart sound, various methodologies rely on time-frequency transforms, including the Short-Time Fourier Transform (STFT), the Wigner-Ville Distribution (WVD), the Smoothed Pseudo-Wigner-Ville Distribution (SPWVD), and the Hilbert Vibration Decomposition (HVD). In this context, Barma et al. [36] proposed an integrated HVD-SPWVD approach for the quantitative evaluation of respiratory splitting [37–39]. This procedure involves decomposing the S2 signal into phase-stable components and applying SPWVD to extract temporal information. The distinction between the aortic and pulmonary components is achieved through averaging and subtraction operations, allowing accurate analysis of split variations in relation to the respiratory cycle [33]. Accurate detection of heart sounds is fundamental for extracting the temporal landmarks required to compute CTIs. In recent years, numerous studies have employed a variety of Deep Learning (DL) and Machine Learning (ML) techniques for heart sound detection and CTIs estimation. Wavelet transforms, such as the Discrete Wavelet Transform (DWT), the Wavelet Packet Transform (WPT), and the Perceptual Wavelet Packet Transform (PWPT), have been used for feature extraction from PCG signals. The study by Behera et al. [40] combined wavelet-based techniques with optimization methods like Neighborhood Component Analysis and ML classifiers, including Support Vector Machine (SVM), k-Nearest Neighbors (KNN), Decision Tree and Random Forest, achieving improved accuracy in the detection of S1 and S2 heart sounds. In the DL domain, feature extraction methods have included time-frequency representations such as Spectrograms, Mel-Frequency Cepstral Coefficients (MFCC) and Chromagrams, which are used as input to Convolutional Neural Networks (CNNs) [41]. An innovative approach has addressed intersubject variability by clustering patients according to age and PCG time-frequency features, combining MFCCs with PCG fragments and classifying them with a Random Forest model [42]. A multimodal integration of ECG and PCG signals into one-dimensional and two-dimensional CNNs has been proposed in [43], with the aim of improving the accuracy of cardiac event detection and the subsequent extraction of clinically relevant parameters.

2.3 Wearable ECG-PCG Devices for Cardiac Monitoring

The growing need for continuous and non-invasive monitoring of cardiovascular diseases has driven the development of a wide range of wearable devices, which integrate various sensors and processing techniques to support prevention and clinical management. The following section presents some representative examples. In [44], a device developed in collaboration

with Ticking Heart is proposed, capable of simultaneously acquiring multichannel PCG signals and ECG to support the prevention of CVD. To improve signal quality, each digital stethoscope integrates a reference microphone dedicated to suppressing ambient noise using a Wiener filter. The device consists of six digital stethoscopes and a three-lead ECG sensor. Furthermore, the study introduces an ML method based on CNNs, aimed at achieving better performance in terms of accuracy and specificity compared to algorithms that analyze PCG signals alone. To date, few studies have explored the use of ECG systems with closely spaced electrodes to obtain standard leads [45]. In a work by Lee et al. [46], the feasibility of a 12-channel ECG based on this configuration has been demonstrated. Building on previous studies that confirmed the feasibility of deriving standard leads from closely spaced ECG electrodes, this principle has been applied in the development of a wearable digital stethoscope patch. The device integrates a single-lead ECG and impedance pneumography, with an inter-electrode distance of 55 mm, designed to provide multimodal analysis for long-term cardiovascular and respiratory monitoring. The experimental pipeline first involved evaluating the estimation of Einthoven's standard leads derived from the device, followed by using the reconstructed ECG to classify fiducial points and the S1 and S2 heart sounds on the PCG acquired by the stethoscope. The extracted information was then used to calculate the PEP and LVET intervals [15]. Numerous recent studies have contributed to the advancement of research in the field of digital sensors for heart sound acquisition. Several technologies have been employed to improve heart sound detection, including arrays of piezoresistive MEMS sensors, piezoelectric elements, flexible sensors, and fiber optic solutions, thereby increasing the sensitivity and reliability of measurements. Despite these advancements, the simultaneous acquisition and synchronization of ECG and PCG signals remains a less explored area [2]. Monteiro et al. [47] proposed a system based on the use of electret microphones and dry polymer electrodes for the joint detection of ECG and PCG. More recently, Cho et al. [48] introduced a wearable device capable of recording both signals in parallel, although electret microphones may introduce limitations in signal fidelity. In Zang et al. [2], the authors introduced a cost-effective and non-invasive solution tailored for widespread usability. The device, based on PZT sensors, enables real-time acquisition of ECG and PCG signals and the subsequent extraction of clinically relevant parameters such as EMD, LVET, and PEP, supporting the early diagnosis of cardiovascular diseases. These developments underscore the growing clinical and technological potential of wearable ECG-PCG systems.

2.4 Approaches to Respiratory Signal Estimation

The assessment of respiration plays a fundamental role in the diagnosis and management of cardiorespiratory diseases [49]. A significant example is the postoperative period, during which respiratory rate can serve as an early indicator of critical events, such as the onset of heart attack [50]. Traditionally, this evaluation has been performed through the direct observation of thoracic and abdominal movements by healthcare personnel, which increases the margin of error and operational costs [49, 51, 52]. Although electronic methods for respiratory monitoring are now available, they often require the use of obstructive devices such as facial masks or nasal cannulas, which can compromise patient comfort and alter the natural breathing pattern. To overcome these limitations, several studies have highlighted the potential of accelerometers as alternative sensors for respiratory signal extraction [51–56]. These devices allow for continuous and non-invasive measurement of respiratory activity while preserving the natural physiology of breathing, an aspect particularly relevant for patients in vulnerable clinical conditions [52, 53]. Various methods

have been developed to estimate respiratory activity using both mechanical and physiological signals. Among them, accelerometer-based approaches provide information on thoracic motion, while biosignal-based methods exploit respiration-induced modulations of cardiovascular signals. The following sections summarize the main developments in these two research domains.

2.4.1 Respiration Estimation from Accelerometric Signals

Among the earliest approaches to non-invasive respiratory monitoring, accelerometers were employed to capture thoracic motion associated with breathing. Hung et al. [57] proposed a method for estimating respiratory rate under static conditions using a biaxial sensor. This approach was later extended to the use of triaxial accelerometers, introducing a method based on hybrid PCA to improve the representation of respiratory movements [58]. However, these spatial acceleration-based methods present significant limitations due to motion artifacts and posture changes, as the acceleration signals induced by movement tend to mask the respiratory component. To overcome these limitations, Liu et al. [59] subsequently proposed a method capable of continuously estimating the breathing waveform, and thus the respiratory rate, even under dynamic conditions, by measuring inclination and variations in thoracic angle during activities characterized by different levels of energy expenditure (EE), such as walking, running, sitting, and sleeping. This approach, based on spectral analysis of the accelerometric signal, demonstrated greater robustness and resilience to artifacts compared to previous methods. Building on these early developments, subsequent research focused on optimizing sensor configuration and signal quality in multi-sensor systems. In this context, the study presented in [60] highlights the importance of defining how the number and placement of sensors influence the SNR, also in relation to individual subject characteristics and different breathing patterns, thereby resulting in variable accuracy of the acquired signals. Starting from this observation, a preliminary analysis is conducted to identify the most effective sensor configuration within a heterogeneous population. The device used consists of a custom-made array of ten accelerometers positioned on the abdomen and chest, whose signals are compared with a reference obtained through a pneumotachographic mask. The second objective of the study concerns the possibility of extracting respiratory information blindly, assuming that the accelerometric signals represent unknown linear combinations of respiration, the source of interest, and other physiological components and artifacts. From this perspective, the output vector is modeled as blind source separation (BSS) problem, for which independent component analysis (ICA) is the most widely used approach. This method is based on the assumption that the various physiological sources, including respiration, are statistically independent, and allows for the estimation of the respiratory component without the use of reference signals obtained, for example, through invasive devices.

2.4.2 Respiration Estimation from Biosignals

In addition to mechanical measurements, respiratory information can also be extracted from physiological signals that reflect cardiorespiratory interactions. Among these, the ECG and photoplethysmogram (PPG) are particularly relevant, as respiration induces characteristic modulations in both electrical and mechanical cardiac activity. These modulations can be exploited to estimate a respiratory waveform or breathing rate without the need for dedicated respiratory sensors. Respiratory signals can be extracted from ECG and PPG signals using either feature-based or filter-based techniques. The influence of respiration on these signals can be classified into three distinct types of modulation [61]:

- **Baseline wander (BW):** In the ECG, this component arises from variations in thoracic impedance and shifts in the electrical axis of the heart relative to the electrodes. In the PPG, it primarily results from changes in peripheral blood volume and vasoconstriction of cutaneous vessels that occur during inspiration.

- **Amplitude modulation (AM):** During inspiration, the reduction in venous return leads to a decrease in stroke volume and, consequently, a reduction in the amplitude of both the QRS complex in the ECG and the pulsatile waveform in the PPG.

- **Frequency modulation (FM):** This modulation originates from RSA, a phenomenon in which HR increases during inspiration and decreases during expiration.

Charlton et al. [61] conducted a systematic study to analyze how technical and physiological factors influence the quality of respiratory signals extracted from ECG and PPG. The main objective was to assess the reliability of the three types of modulation (AM, FM, and BW) in reconstructing a respiratory signal and estimating respiratory rate across different contexts. The results showed that the quality of the extracted signal depends on multiple variables: technical factors, such as the choice of source signal (ECG or PPG), and physiological factors, such as age or the presence of arrhythmias. In particular, FM was found to be less reliable in elderly subjects, as RSA tends to diminish or disappear with age. Moreover, the authors observed that the quality of most respiratory signals decreases at higher respiratory rates, indicating a general decline in estimation accuracy. The study therefore emphasized that the robustness of extraction techniques is strongly dependent on the subject's physiological condition and the measurement context. A more recent evolution in respiratory signal extraction methods is represented by the study of Miao et al. [62], which proposes an end-to-end model called RespDiff for estimating the respiratory waveform from PPG signals. This approach introduces, for the first time, the application of diffusion models to respiratory signal analysis, combined with a multi-scale Recurrent Neural Network (RNN) architecture capable of capturing respiratory modulations distributed across different frequency bands. Additionally, a spectral loss is integrated to optimize signal reconstruction in the frequency domain. Validated on the BIDMC dataset [63], the model demonstrated superior performance compared to traditional methods, showing greater robustness even in the presence of noise or signal quality variations. This study highlights how the integration of generative models and recurrent neural networks represents a promising direction for continuous and non-invasive respiratory signal estimation.

2.5 Effect of Respiratory Phase on CTI Accuracy

It is essential to understand the physiological effects of respiration on heart sounds, as the pressure and volume variations, induced by the respiratory cycle, influence both the morphology and timing of cardiac mechanical events. Variations in heart sounds reflect the influence of respiration on the timing of cardiac valve closure, mediated by changes in intrathoracic pressure and venous return dynamics, which affect ventricular filling. During inspiration, the reduction in intrathoracic pressure caused by the expansion of the thoracic cavity promotes blood flow to the right ventricle, resulting in delayed closure of the pulmonary valve and earlier closure of the aortic valve. This phenomenon leads to an increase in the splitting of the second heart sound. During expiration, the opposite process occurs: venous return decreases and the two components tend to merge [33]. The physiological split of the second heart sound thus serves as an indicator of the hemodynamic variations that occur throughout the respiratory cycle. Regarding the first heart sound, the study conducted by Tang et al. (2015) [32] showed that the delay in S1 progressively increases during

inspiration, reaching its maximum at the end of this phase, and decreases during expiration. Respiratory-induced variations in the preload and afterload of the ventricular affect the temporal relationship between electrical activation and the mechanical response of the myocardium, altering both the morphology and timing of heart sounds. In a quantitative study modeling heart sounds as a sum of Gaussian curves, morphological variations were analyzed in terms of amplitude, timing, and supporting width. The amplitude of S2 was found to increase during inspiration and diminish during expiration, while no consistent trend was observed for S1. Additionally, the supporting width of S1 increased during inspiration and decreased during expiration, reflecting the mechanical impact of intrathoracic pressure fluctuations on valve dynamics. The delay span of S2 was often found to be greater than that of S1, suggesting that respiratory activity exerts a stronger modulation on the mechanical events associated with semilunar valve closure. These cyclic morphological changes confirm the high sensitivity of cardiac sounds to respiration-induced hemodynamic variations, providing a non-invasive window into cardiorespiratory coupling [35].Several studies have shown that respiratory phases modulate CTIs. In particular, an increase in PEP and a reduction in LVET are observed during inspiration, both at rest and after physical exercise [64]. This behavior can be explained by the decrease in pleural pressure that occurs during inspiration, which leads to a relative increase in aortic pressure and, consequently, in afterload. This effect causes a delay in mitral valve closure and aortic valve opening, thereby prolonging PEP. During expiration, the opposite process occurs: reduction in afterload shortens PEP and prolongs ejection time [65]. These findings confirm that respiration-induced hemodynamic variations systematically affect the timing of mechanical cardiac events and, as a result, may compromise the accuracy of CTI estimation if the respiratory phase is not explicitly taken into account.

2.6 Open Challenges in the Interaction Between Respiratory and Cardiovascular Signals

Interactions between the respiratory and cardiovascular systems represent a complex and dynamic phenomenon, still under investigation due to its nonlinear nature and the challenges associated with accurate modeling. Respiratory modulations simultaneously affect electrical, mechanical, and hemodynamic parameters of the heart, leading to variations in frequency, morphology, and timing of cardiac events. However, the cardiorespiratory response exhibits high interindividual variability and depends on several factors, such as respiratory rate, breath depth, and the subject's autonomic state. This complexity makes it difficult to isolate the direct effects of respiration on cardiovascular signals and poses a significant challenge for the quantitative analysis and modeling of heart-lung coupling. Although recent studies have demonstrated the feasibility of estimating respiratory and cardiac parameters using non-invasive devices based on biosignal acquisition, several challenges remain in ensuring robust and reliable monitoring of cardiorespiratory interactions in real-time and over extended periods. One of the main limitations is the presence of motion artifacts, which inevitably degrade signal quality. Body movements, postural changes, or even speech, difficult to control in a home environment compared to experimental settings, can introduce non-physiological fluctuations that obscure subtle respiratory modulations, leading to erroneous segmentation of mechanical events and, consequently, inaccurate estimation of CTIs. Another critical issue arises form irregular heart rhythms, such as arrhythmias, which introduce additional variability and pose significant challenges to algorithms based on regular beat-to beat cadence. The normal physiological coupling between respiration and cardiac dynamics may thus be disrupted, reducing the coherence of features dependent on respiratory phase. The impact of such variability on the accuracy and robustness of

respiration-dependent CTI estimation remains an open question, particularly regarding the system's adaptability to different physiological conditions. In light of these challenges, further developments are needed toward advanced signal processing techniques and intelligent artifact management, in order to enhance the clinical effectiveness of non-invasive devices in home-based settings. Future research may focus on integrating data from accelerometers or gyroscopes, implementing adaptive filtering techniques, and employing ML and DL approaches equipped with personalized calibration phases, thereby optimizing monitoring performance and ensuring greater long-term reliability [41].

Chapter 3

Materials and Methods

3.1 Description of the Wearable Device

The wearable system used in this study was specifically developed to enable the simultaneous acquisition of ECG, PCG, and accelerometric signals. The multimodal configuration was designed to investigate the interaction between electrical, mechanical, and acoustic cardiac activity and to extract respiratory information from chest motion. The core component of the device consists of a flexible array that conforms to the subject's left hemithorax. The array integrates 48 electret condenser microphones for PCG acquisition and three electrodes for single-lead ECG recording. The dense spatial distribution of the microphones allows users with no prior experience in auscultation to perform high-quality recordings without assistance from clinical or technical personnel. A detailed description of the device design is provided in [66]. A miniaturized magneto-inertial measurement unit (MIMU) is positioned on top of the array, over the sternal area, to capture 3D chest wall accelerations. This configuration allows the detection of both cardiac-induced microvibrations and respiratory-induced movements. The inertial data are processed by an onboard floating-point microcontroller. The ECG/PCG array and the MIMU system operate asynchronously. To achieve precise temporal alignment, cross-correlation between PCG and accelerometric signals filtered within the heart sound bandwidth (20–100 Hz) was performed. All signals were resampled to 1 kHz for further analysis.

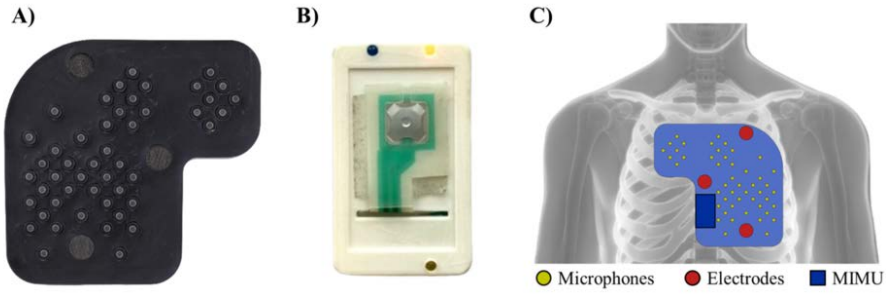

Figure 3.1. Configuration of the acquisition system. A) Setup for ECG and PCG signal collection. B) Inertial sensor (MIMU) for measuring chest wall accelerations. C) Placement of the sensing elements on the thoracic surface [66].

3.2 Data Acquisition Protocol

Twelve healthy volunteers (5 females) participated in the data acquisition sessions. All participants reported no history of cardiovascular or respiratory diseases and no ongoing medication that could influence cardiac or respiratory activity. The inclusion of healthy subjects was considered appropriate to perform a preliminary evaluation of whether incorporating respiratory signal analysis could improve the accuracy of cardiac time interval estimation. Each participant was fitted with the acquisition device using an adjustable vest-like belt designed to ensure stable sensor positioning according to individual body shape. Data were collected with subjects lying in a supine position on an examination bed, instructed to remain still and breathe spontaneously without any imposed rhythm or verbal cue, to preserve natural respiratory patterns. For each subject, a single recording of 60 seconds was acquired. The participants had a median age of 25 years (range: 24–70 years). Although the sample size is limited, the study can be regarded as a pilot investigation aimed at assessing the feasibility and consistency of the proposed approach.

Table 3.1. Anthropometric characteristics of the participants.

Subject ID	**Age**	**Gender**	**Height (m)**	**Weight (kg)**	**BMI (kg m^{-2})**
subj_01	–	–	–	–	–
subj_02	–	–	–	–	–
subj_03	70	M	1.77	76	24.3
subj_04	25	M	1.83	83	24.8
subj_05	25	F	1.67	55	19.7
subj_06	24	M	1.90	90	24.9
subj_07	28	F	1.60	50	19.5
subj_08	24	M	1.80	70	21.6
subj_09	26	M	1.76	71	22.9
subj_10	24	M	1.74	59	19.5
subj_11	25	F	1.64	66	24.5
subj_12	25	M	1.78	71	22.4

3.3 Methods for Estimating the Respiratory Signal

Respiratory information was estimated from three physiological signals recorded simultaneously: acceleration, ECG, and PCG. Each of these signals contains respiration-related components arising from distinct physiological mechanisms, such as mechanical chest wall motion in the acceleration signal, RSA in the ECG, and variations in cardiac sounds in the PCG. To minimize transient artifacts, the initial second of each recording was excluded from analysis, as identified through visual inspection of the dataset. A specific method was implemented for each signal to extract the corresponding respiratory information. A processing pipeline was adopted for all signal sources in order to ensure respiratory signals of good quality, with reduced noise levels and methodological consistency across the different extraction modalities. This section describes the signal-specific extraction procedures (Sections 3.3.1–3.3.3) and the shared processing steps used to obtain the final respiratory waveforms (Section 3.3.4).

3.3.1 Accelerometer-derived respiration

The respiratory signal was derived from the triaxial accelerometer positioned on the sternum, which captures the mechanical expansion and contraction of the thoracic wall during breathing. Before processing, the mean value of each acceleration axis was removed to eliminate the direct current (DC) component. The three acceleration components were then combined into a single magnitude signal by computing the Euclidean norm:

$$a_{\text{norm}}(t) = \sqrt{a_x^2(t) + a_y^2(t) + a_z^2(t)}. \tag{3.1}$$

The use of the vector norm, instead of a single-axis signal, was preferred as it improves the sensitivity of the device in capturing chest wall motion due to respiration [67]. This approach is consistent with the findings of Lin and Jhou [68], who applied wavelet analysis to extract respiratory frequency from seismocardiogram signals recorded by MEMS triaxial accelerometers in a supine posture, achieving a remarkably low estimation error of 0.0035 ± 0.0628 Hz (0.21 ± 3.77 bpm in RR). These results confirm the feasibility of respiratory rate estimation from accelerometric signals under controlled postural conditions. Furthermore, previous studies have shown that no significant differences are typically observed among orthogonal acceleration directions, supporting the use of combined-axis representations to improve robustness across varying postures and sensor placements [69]. The resulting norm signal was then downsampled to the target frequency to reduce computational load before the application of the subsequent processing steps described in Section (3.3.4).

3.3.2 ECG-derived respiration

Accurate detection of R-peaks is therefore essential to ensure the reliability of the continuously reconstructed respiratory signal derived from the ECG. R-peaks were detected using an implementation of the Pan–Tompkins algorithm [70], originally developed for QRS detection in ECG signals and subsequently adapted to the characteristics of the acquired dataset. The modifications aimed to improve detection robustness under the specific experimental conditions and to enable its integration into a fully automated processing pipeline without graphical user interfaces. In particular, the algorithm was refined through: (i) recentring of each R-peak on the local maximum within ± 40 ms; (ii) polarity check and signal inversion, when necessary, to ensure consistency of peak orientation; (iii) enforcement of a minimum refractory period of 0.35 s, suitable for resting subjects in semi-recumbent position; and (iv) removal of low-amplitude detections below 30% of the median peak value. These parameter values were established empirically based on the inspection of the acquired ECG recordings. The resulting sequence of R-peak locations was then used to derive two respiratory signals based on temporal and morphological modulations of the ECG.

RR-based extraction

The first respiratory estimate was obtained from the beat-to-beat variability of the cardiac period. Consecutive R–R intervals were computed from the sequence of detected R-peaks, and the resulting series was interpolated to obtain a uniformly sampled, continuous respiratory waveform. This approach exploits the well-known coupling between respiration and heart rate, known as RSA, where breathing modulates the cardiac cycle length.

Amplitude-based extraction

A second respiratory estimate was derived from respiratory-induced modulations of the QRS complex amplitude, following the method proposed [71]. For each detected R-peak, the corresponding S-wave was identified as the minimum value of the ECG within a 0.1 s window following the R-peak, and the R–S amplitude difference was computed. The resulting sequence of R–S amplitudes reflects respiration-related morphological variations of the ECG and was used to generate an additional respiratory waveform.

Both derived time series were subsequently processed using the common pipeline described in Section(3.3.4).

3.3.3 PCG-derived respiration

Based on the physiological mechanisms underlying the generation of the S1 and S2 heart sounds (see Section 2.2), both components were analyzed to assess respiration-induced modulations in cardiac timing. The extraction was performed separately for S1 and S2, in order to evaluate which component provided a more robust respiratory estimate.

S1-based extraction
The respiratory signal was first extracted from S1, associated with the closure of the atrioventricular valves. Each PCG channel was band-pass filtered in the 20–100 Hz range using a Chebyshev type II filter to isolate the frequency content corresponding to the main heart sounds. The Shannon energy envelope was then computed to enhance the SNR and facilitate the detection of S1 peaks. For each cardiac cycle, S1 peaks were identified within the first 20% of the R–R interval following each R-peak in the ECG. The sequence of detected S1 events was used to compute the S1–S1 intervals, which reflect the respiration-induced variability of cardiac timing. These intervals were interpolated to obtain a continuous respiratory waveform representing the slow modulation of heart sound timing associated with the breathing activity.

S2-based extraction
A similar procedure was applied to extract the respiratory signal from S2, related to the closure of the semilunar valves. S2 peaks were identified within the 30–60% portion of each R–R interval, based on the corresponding ECG R-peak timing. For each PCG channel, the sequence of S2 occurrences was used to compute the S2–S2 intervals, capturing the respiratory influence on the temporal spacing of cardiac sounds. The resulting interval series was interpolated to generate a continuous respiratory waveform, following the same procedure applied for S1.

Quality metrics and channel selection
To assess the reliability of the extracted signals, the SNR was computed for each PCG channel following the formulation proposed by [72]. The SNR was defined as:

$$\mathrm{SNR} = 20 \log_{10} \left(\frac{A_S}{4\sigma_N} \right), \tag{3.2}$$

where A_S represents the peak-to-peak amplitude of the mean cardiac cycle, and σ_N is the standard deviation of the noise estimated within the 70–85% portion of the mean cycle, where no heart sounds are expected. The channel with the highest SNR was automatically selected for further analysis, and its corresponding respiratory signal was retained for comparison with the other modalities (Section 3.3.4).

3.3.4 Cardiac latency–derived respiration

The respiratory signal was also estimated from the beat-to-beat variations in the timing of cardiac valve events, quantified as the latencies between the R-wave of the ECG and the main heart sound components, namely the mitral (S_{1m}) and tricuspid (S_{1t}) components of S1, and the aortic (S_{2a}) and pulmonary (S_{2p}) components of S2. ECG and PCG signals were processed using algorithms previously developed and validated by [72]. The ECG was band-pass filtered (10–35 Hz) through the cascade of two 250th-order FIR filters to remove baseline drift and high-frequency noise, and R-peaks were detected using a modified version of the Pan–Tompkins algorithm. The PCG signals were band-pass filtered between 20

and 100 Hz using a fifth-order Chebyshev IIR filter applied in a zero-phase configuration. Heart sounds were segmented using the second-order Shannon energy envelope, followed by amplitude and time thresholding for the detection of S_1 and S_2 components, allowing the identification of their subcomponents as described in [72]. For each cardiac cycle, the temporal latencies between the R-wave and the corresponding valvular components were computed and subsequently converted from milliseconds to seconds to ensure unit consistency across all derived signals. The resulting beat-to-beat latency series constituted the discrete basis for constructing the respiratory waveforms, as described in the following section.

3.3.5 Common Processing Pipeline

After the extraction of respiration-related series from each modality, a common processing pipeline was applied to obtain continuous, temporally aligned respiratory waveforms suitable for comparison across methods. All signals were first interpolated and resampled at a uniform frequency of 25 Hz, ensuring consistent temporal resolution and facilitating subsequent analyses. The piecewise cubic Hermite interpolation (pchip) method was selected after evaluating different interpolation schemes commonly used for physiological signals. Linear interpolation offers computational simplicity and avoids spurious oscillations but can introduce abrupt slope discontinuities that may distort the temporal morphology of respiratory cycles. Spline interpolation provides higher-order smoothness and visually continuous profiles; however, its tendency to overshoot between samples can generate artificial peaks and troughs, which are undesirable when the accurate delineation of respiratory cycles is required. Pchip represents a compromise between these two approaches, preserving the monotonicity and overall shape of the signal while ensuring smooth, physiologically consistent transitions. This balance makes it particularly suitable for obtaining realistic respiratory waveforms and reliable estimation of cycle boundaries and respiratory rate. A 10 s moving average was applied and subtracted from each respiratory estimate to remove slow baseline trends and low-frequency fluctuations unrelated to breathing. The window length was selected to effectively suppress very slow variations while maintaining the typical frequency content associated with normal respiratory activity in healthy awake adults at rest. This operation further mitigates low-frequency variations arising from slow postural adjustments, mechanical instabilities, or gradual physiological changes that can introduce non-respiratory modulations across all sensing modalities. Finally, a zero-phase low-pass Chebyshev type II filter of seventh order was applied, with a stopband attenuation of 50 dB and a normalized cutoff frequency of 0.5 Hz (corresponding to the upper limit of the expected respiratory band). This filtering stage preserved the morphology of the respiratory waveform while reducing high-frequency fluctuations and residual cardiac components. The resulting signals represent the continuous respiratory waveforms derived from each source, used for all subsequent analyses and comparisons.

3.4 Identification of Respiratory Phases and Characteristic Points

The segmentation of the respiratory signal into inspiratory and expiratory phases was performed by identifying local maxima and minima using a Zero-Crossing with Amplitude Threshold (ZC-AT) algorithm derived from Khodadad et al. [73]. The algorithm analyzes the zero-crossings of the signal to alternately detect end-expiration points (minima) and end-inspiration points (maxima). Each potential extremum is validated based on two temporal criteria: the interval between consecutive crossings with the same slope, defined as

Identical Crossing Spacing (ICS), and the interval between consecutive crossings with opposite slopes, defined as Different Crossing Spacing (DCS). The extrema are accepted only if both intervals exceed minimum thresholds, namely Minimum Identical Crossing Spacing (MICS) and Minimum Different Crossing Spacing (MDCS), calculated as:

$$\mathrm{MICS} = \mathrm{MICS}_{\mathrm{fact}} \cdot \frac{60}{\mathrm{maxBR}}, \qquad \mathrm{MDCS} = \mathrm{MDCS}_{\mathrm{fact}} \cdot \frac{60}{\mathrm{maxBR}}$$

where $\mathrm{MICS}_{\mathrm{fact}}$ and $\mathrm{MDCS}_{\mathrm{fact}}$ are dimensionless factors scaling the temporal thresholds relative to the maximum respiratory rate (maxBR), fixed at 150 breaths/min. This value was kept consistent with the original formulation of [73], where it serves as a theoretical limit for temporal normalization and does not represent a physiological value for adult subjects. To reduce false detections caused by small-amplitude oscillations or noise, an additional amplitude-based validation criterion was introduced. The minimum acceptance threshold, referred to as Low Tidal Amplitude (lowTA), is defined as:

$$\mathrm{lowTA} = \mathrm{typTA} \cdot \mathrm{lowTA}_{\mathrm{fact}}$$

where typTA (Typical Tidal Amplitude) represents the typical tidal amplitude, corresponding to the 80th percentile of the respiratory amplitude distribution, and $\mathrm{lowTA}_{\mathrm{fact}}$ is a coefficient between 0 and 1 defining the minimum fraction of the typical amplitude required for a cycle to be considered valid. The parameters $\mathrm{MICS}_{\mathrm{fact}}$, $\mathrm{MDCS}_{\mathrm{fact}}$, and $\mathrm{lowTA}_{\mathrm{fact}}$ were initially explored within the following validity ranges:

$$\mathrm{MICS}_{\mathrm{fact}} \in [0.5, 0.75], \quad \mathrm{MDCS}_{\mathrm{fact}} \in [0.1, 0.25], \quad \mathrm{lowTA}_{\mathrm{fact}} \in [0.1, 0.9]$$

The parameter configurations were considered acceptable only if they produced physiological respiratory rates for awake, resting adults (6–20 breaths/min) and at least five coherent respiratory cycles. Respiratory rates within this range were considered physiologically plausible, as slower frequencies (6–11 breaths/min) that have been shown to enhance vagal power by entraining cardiac activity to the respiratory rhythm, thereby strengthening parasympathetic modulation [74], while typical spontaneous breathing in healthy adults falls between 12 and 20 breaths/min, with 90% of values reported within 11.8–19.2 breaths/min [75]. The analysis showed a stable convergence toward $\mathrm{MICS}_{\mathrm{fact}} = 0.50$ and $\mathrm{MDCS}_{\mathrm{fact}} = 0.10$, in agreement with the values originally proposed by [73]. The parameter $\mathrm{lowTA}_{\mathrm{fact}}$ exhibited greater variability, but the choice of 0.10 proved to be the most balanced, as it preserved the physiological plausibility of the respiratory rate while maintaining the inclusion of low-amplitude cycles. The final parameter values and their respective exploration ranges are reported in Table 3.2.

Table 3.2. Explored ranges and final values of the parameters used for respiratory signal segmentation

Parameter	Description	Explored range	Final value
$\mathrm{MICS}_{\mathrm{fact}}$	Scaling factor for the ICS threshold	[0.5, 0.75]	0.50
$\mathrm{MDCS}_{\mathrm{fact}}$	Scaling factor for the DCS threshold	[0.1, 0.25]	0.10
$\mathrm{lowTA}_{\mathrm{fact}}$	Minimum fraction of the typical tidal amplitude required for a valid cycle	[0.1, 0.9]	0.10

3.5 Estimation of Cardiac Latencies with Respect to the Respiratory Cycle

Bibliography

[1] Muthiah Vaduganathan, George A. Mensah, Justine Varieur Turco, Valentin Fuster, and Gregory A. Roth. The global burden of cardiovascular diseases and risk. *Journal of the American College of Cardiology*, 80(25):2361–2371, December 2022.

[2] Junbin Zang, Qi An, Bo Li, Zhidong Zhang, Libo Gao, and Chenyang Xue. A novel wearable device integrating ecg and pcg for cardiac health monitoring. *Microsystems amp; Nanoengineering*, 11(1), January 2025.

[3] Anuradha Lala, Craig Beavers, Vanessa Blumer, Laprincess Brewer, Diana De Oliveira-Gomes, Sandra B. Dunbar, Hannah Every, Richard Ferraro, Bonnie Ky, James L. Januzzi, Francoise Marvel, Robert J. Mentz, Erin Michos, Jagat Narula, Khuram Nasir, Pradeep Natarajan, Lori Ann Peterson, Fatima Rodriguez, Michael D. Shapiro, Jenna Skowronski, Randall C. Starling, Pam Taub, Ryan J. Tedford, Quentin Youmans, Shelley Zieroth, and Martha Gulati. The continuum of prevention and heart failure in cardiovascular medicine: A joint scientific statement from the heart failure society of america and the american society for preventive cardiology. *Journal of Cardiac Failure*, August 2025.

[4] Theresa A McDonagh, Marco Metra, Marianna Adamo, Roy S Gardner, Andreas Baumbach, Michael Böhm, Haran Burri, Javed Butler, Jelena Čelutkienė, Ovidiu Chioncel, John G F Cleland, Andrew J S Coats, Maria G Crespo-Leiro, Dimitrios Farmakis, Martine Gilard, Stephane Heymans, Arno W Hoes, Tiny Jaarsma, Ewa A Jankowska, Mitja Lainscak, Carolyn S P Lam, Alexander R Lyon, John J V McMurray, Alexandre Mebazaa, Richard Mindham, Claudio Muneretto, Massimo Francesco Piepoli, Susanna Price, Giuseppe M C Rosano, Frank Ruschitzka, Anne Kathrine Skibelund, Rudolf A de Boer, P Christian Schulze, Magdy Abdelhamid, Victor Aboyans, Stamatis Adamopoulos, Stefan D Anker, Elena Arbelo, Riccardo Asteggiano, Johann Bauersachs, Antoni Bayes-Genis, Michael A Borger, Werner Budts, Maja Cikes, Kevin Damman, Victoria Delgado, Paul Dendale, Polychronis Dilaveris, Heinz Drexel, Justin Ezekowitz, Volkmar Falk, Laurent Fauchier, Gerasimos Filippatos, Alan Fraser, Norbert Frey, Chris P Gale, Finn Gustafsson, Julie Harris, Bernard Iung, Stefan Janssens, Mariell Jessup, Aleksandra Konradi, Dipak Kotecha, Ekaterini Lambrinou, Patrizio Lancellotti, Ulf Landmesser, Christophe Leclercq, Basil S Lewis, Francisco Leyva, Aleš Linhart, Maja-Lisa Løchen, Lars H Lund, Donna Mancini, Josep Masip, Davor Milicic, Christian Mueller, Holger Nef, Jens-Cosedis Nielsen, Lis Neubeck, Michel Noutsias, Steffen E Petersen, Anna Sonia Petronio, Piotr Ponikowski, Eva Prescott, Amina Rakisheva, Dimitrios J Richter, Evgeny Schlyakhto, Petar Seferovic, Michele Senni, Marta Sitges, Miguel Sousa-Uva, Carlo G Tocchetti, Rhian M Touyz, Carsten Tschoepe, Johannes Waltenberger, Marianna Adamo, Andreas Baumbach, Michael Böhm, Haran Burri, Jelena Čelutkienė, Ovidiu Chioncel, John G F Cleland, Andrew J S Coats, Maria G Crespo-Leiro, Dimitrios Farmakis, Roy S Gardner, Martine Gilard, Stephane Heymans, Arno W Hoes, Tiny Jaarsma, Ewa A Jankowska, Mitja Lainscak, Carolyn S P Lam, Alexander R Lyon, John J V McMurray, Alexandre

Mebazaa, Richard Mindham, Claudio Muneretto, Massimo Francesco Piepoli, Susanna Price, Giuseppe M C Rosano, Frank Ruschitzka, and Anne Kathrine Skibelund. 2021 esc guidelines for the diagnosis and treatment of acute and chronic heart failure. *European Heart Journal*, 42(36):3599–3726, August 2021.

[5] M. S. Nieminen, D. Brutsaert, K. Dickstein, H. Drexler, F. Follath, V.-P. Harjola, M. Hochadel, M. Komajda, J. Lassus, J. L. Lopez-Sendon, P. Ponikowski, and L. Tavazzi. Euroheart failure survey ii (ehfs ii): a survey on hospitalized acute heart failure patients: description of population. *European Heart Journal*, 27(22):2725–2736, April 2006.

[6] Òscar Miró, Ana García Sarasola, Carolina Fuenzalida, Sofía Calderón, Javier Jacob, Alfons Aguirre, Da M. Wu, Miguel A. Rizzi, Pierre Malchair, Antonio Haro, Sergio Herrera, Víctor Gil, Francisco J. Martín-Sánchez, Pere Llorens, Pablo Herrero Puente, Héctor Bueno, Alberto Domínguez Rodríguez, Christian E. Müller, Alexandre Mebazaa, Ovidiu Chioncel, and Aitor Alquézar-Arbé. Departments involved during the first episode of acute heart failure and subsequent emergency department revisits and rehospitalisations: an outlook through the novica cohort. *European Journal of Heart Failure*, 21(10):1231–1244, August 2019.

[7] Jawad H. Butt, Emil L. Fosbøl, Thomas A. Gerds, Charlotte Andersson, John J.V. McMurray, Mark C. Petrie, Finn Gustafsson, Christian Madelaire, Søren Lund Kristensen, Gunnar H. Gislason, Christian Torp-Pedersen, Lars Køber, and Morten Schou. Readmission and death in patients admitted with new-onset versus worsening of chronic heart failure: insights from a nationwide cohort. *European Journal of Heart Failure*, 22(10):1777–1785, March 2020.

[8] Patricia Javaloyes, Òscar Miró, Víctor Gil, Francisco Javier Martín-Sánchez, Javier Jacob, Pablo Herrero, Koji Takagi, Aitor Alquézar-Arbé, María Pilar López Díez, Enrique Martín, Carlos Bibiano, Rosa Escoda, Cristina Gil, Marta Fuentes, Guillermo Llopis García, José María Álvarez Pérez, Alba Jerez, Josep Tost, Lluís Llauger, Rodolfo Romero, José Manuel Garrido, Esther Rodríguez-Adrada, Carolina Sánchez, Xavier Rossello, John Parissis, Alexandre Mebazaa, Ovidiu Chioncel, and Pere Llorens. Clinical phenotypes of acute heart failure based on signs and symptoms of perfusion and congestion at emergency department presentation and their relationship with patient management and outcomes. *European Journal of Heart Failure*, 21(11):1353–1365, June 2019.

[9] Josef Stehlik, Carsten Schmalfuss, Biykem Bozkurt, Jose Nativi-Nicolau, Peter Wohlfahrt, Stephan Wegerich, Kevin Rose, Ranjan Ray, Richard Schofield, Anita Deswal, Jadranka Sekaric, Sebastian Anand, Dylan Richards, Heather Hanson, Matthew Pipke, and Michael Pham. Continuous wearable monitoring analytics predict heart failure hospitalization: The link-hf multicenter study. *Circulation: Heart Failure*, 13(3), March 2020.

[10] Parastoo Dehkordi, Farzad Khosrow-Khavar, Marco Di Rienzo, Omer T. Inan, Samuel E. Schmidt, Andrew P. Blaber, Kasper Sørensen, Johannes J. Struijk, Vahid Zakeri, Prospero Lombardi, Md. Mobashir H. Shandhi, Mojtaba Borairi, John M. Zanetti, and Kouhyar Tavakolian. Comparison of different methods for estimating cardiac timings: A comprehensive multimodal echocardiography investigation. *Frontiers in Physiology*, 10, August 2019.

[11] H. Boudoulas. Systolic time intervals. *European Heart Journal*, 11(suppl I):93–104, January 1990.

[12] P. Reant, M. Dijos, E. Donal, A. Mignot, P. Ritter, P. Bordachar, P. Dos Santos, C. Leclercq, R. Roudaut, G. Habib, and S. Lafitte. Systolic time intervals as simple echocardiographic parameters of left ventricular systolic performance: correlation with ejection fraction and longitudinal two-dimensional strain. *European Journal of*

Echocardiography, 11(10):834–844, July 2010.

[13] Oddbjørn Brubakk, Terje R. Pedersen, and Kåre Overskeid. Noninvasive evaluation of the effect of timolol on left ventricular performance after myocardial infarction and the consequence for prognosis. *Journal of the American College of Cardiology*, 9(1):155–160, January 1987.

[14] Kouhyar Tavakolian, Guy A. Dumont, Geoffrey Houlton, and Andrew P. Blaber. Precordial vibrations provide noninvasive detection of early-stage hemorrhage. *Shock*, 41(2):91–96, February 2014.

[15] Michael Klum, Mike Urban, Timo Tigges, Alexandru-Gabriel Pielmus, Aarne Feldheiser, Theresa Schmitt, and Reinhold Orglmeister. Wearable cardiorespiratory monitoring employing a multimodal digital patch stethoscope: Estimation of ecg, pep, lvet and respiration using a 55 mm single-lead ecg and phonocardiogram. *Sensors*, 20(7):2033, April 2020.

[16] John Kreit. Respiratory-cardiovascular interactions during mechanical ventilation: Physiology and clinical implications, April 2022.

[17] page 279–308. Elsevier, 2022.

[18] R. A. Wise, J. L. Robotham, and W. R. Summer. Effects of spontaneous ventilation on the circulation. *Lung*, 159(1):175–186, December 1981.

[19] Sheldon Magder. Heart-lung interaction in spontaneous breathing subjects: the basics. *Annals of Translational Medicine*, 6(18):348–348, September 2018.

[20] François Feihl and Alain F. Broccard. Interactions between respiration and systemic hemodynamics. part i: basic concepts. *Intensive Care Medicine*, 35(1):45–54, September 2008.

[21] Fumihiko Yasuma and Jun-ichiro Hayano. Respiratory sinus arrhythmia. *Chest*, 125(2):683–690, February 2004.

[22] Maja Elstad, Erin L. O'Callaghan, Alex J. Smith, Alona Ben-Tal, and Rohit Ramchandra. Cardiorespiratory interactions in humans and animals: rhythms for life. *American Journal of Physiology-Heart and Circulatory Physiology*, 315(1):H6–H17, July 2018.

[23] Cheng Xiefeng, Yue Wang, Shicheng Dai, Pengjun Zhao, and Qifa Liu. Heart sound signals can be used for emotion recognition. *Scientific Reports*, 9(1), April 2019.

[24] Zhu Yongbo, Xu Lijun, and Issah Abubakari Samori. Mechanical vibration monitoring system for electrocardiogram machine based on hilbert-huang transformations. *The Journal of Engineering*, 2022(11):1104–1113, October 2022.

[25] Zhixing Gao, Yuqi Wang, Xingchen Xu, Chaohong Zhang, Zhiwei Dai, Haiying Zhang, Jun Zhang, and Hao Yang. A portable cardiac dynamic monitoring system in the framework of electro-mechano-acoustic mapping. *IEEE Transactions on Biomedical Circuits and Systems*, page 1–17, 2024.

[26] Shuenn-Yuh Lee, Peng-Wei Huang, Jia-Ren Chiou, Chieh Tsou, Yu-Yi Liao, and Ju-Yi Chen. Electrocardiogram and phonocardiogram monitoring system for cardiac auscultation. *IEEE Transactions on Biomedical Circuits and Systems*, 13(6):1471–1482, December 2019.

[27] Ramith Hettiarachchi, Udith Haputhanthri, Kithmini Herath, Hasindu Kariyawasam, Shehan Munasinghe, Kithmin Wickramasinghe, Duminda Samarasinghe, Anjula De Silva, and Chamira U. S. Edussooriya. A novel transfer learning-based approach for screening pre-existing heart diseases using synchronized ecg signals and heart sounds. In *2021 IEEE International Symposium on Circuits and Systems (ISCAS)*, page 1–5. IEEE, May 2021.

[28] A.A. Luisada, C.K. Liu, C. Aravanis, M. Testelli, and J. Morris. On the mechanism of production of the heart sounds. *American Heart Journal*, 55(3):383–399, March 1958.

[29] P. M. Shah, M. Mori, D. M. Maccanon, and A. A. Luisada. Hemodynamic correlates of the various components of the first heart sound. *Circulation Research*, 12(4):386–392,

April 1963.

[30] Tsuguya Sakamoto, Reizo Kusukawa, Donald M. Maccanon, Aldo A. Luisada, and Ivan Harvey. Hemodynamic determinants of the amplitude of the first heart sound. *Circulation Research*, 16(1):45–57, January 1965.

[31] T. Sakamoto, R. Kusukawa, D. M. MacCanon, and A. A. Luisada. First heart sound amplitude in experimentally induced alternans. *Chest*, 50(5):470–475, 1966.

[32] Hong Tang, Yongwan Park, and Chengjie Ruan. Nonlinear time domain relation between respiratory phase and timing of the first heart sound. *Computational and Mathematical Methods in Medicine*, 2015:1–7, 2015.

[33] Hong Tang, Huaming Chen, and Ting Li. Discrimination of aortic and pulmonary components from the second heart sound using respiratory modulation and measurement of respiratory split. *Applied Sciences*, 7(7):690, July 2017.

[34] Guy Amit, Khuloud Shukha, Noam Gavriely, and Nathan Intrator. Respiratory modulation of heart sound morphology. *American Journal of Physiology-Heart and Circulatory Physiology*, 296(3):H796–H805, March 2009.

[35] Hong Tang, Jiao Gao, Chengjie Ruan, Tianshuang Qiu, and Yongwan Park. Modeling of heart sound morphology and analysis of the morphological variations induced by respiration. *Computers in Biology and Medicine*, 43(11):1637–1644, November 2013.

[36] Shovan Barma, Bo-Wei Chen, Ka Lok Man, and Jhing-Fa Wang. Quantitative measurement of split of the second heart sound (s2). *IEEE/ACM Transactions on Computational Biology and Bioinformatics*, 12(4):851–860, July 2015.

[37] Michael Feldman. *Hilbert Transform Applications in Mechanical Vibration*. Wiley, March 2011.

[38] Francois Auger, Patrick Flandrin, Yu-Ting Lin, Stephen McLaughlin, Sylvain Meignen, Thomas Oberlin, and Hau-Tieng Wu. Time-frequency reassignment and synchrosqueezing: An overview. *IEEE Signal Processing Magazine*, 30(6):32–41, 2013.

[39] F. Auger and P. Flandrin. Improving the readability of time-frequency and time-scale representations by the reassignment method. *IEEE Transactions on Signal Processing*, 43(5):1068–1089, 1995.

[40] Sukant Behera, Iti Saha Misra, and Khawer Naveed Siddiqui. Phonocardiogram signal based better prediction of aortic and mitral stenosis heart diseases using machine learning. In *2025 International Conference on Ambient Intelligence in Health Care (ICAIHC)*, page 1–6. IEEE, January 2025.

[41] Roberto De Fazio, Ilaria Cascella, Şule Esma Yalçınkaya, Massimo De Vittorio, Luigi Patrono, Ramiro Velazquez, and Paolo Visconti. Synchronous acquisition and processing of electro- and phono-cardiogram signals for accurate systolic times' measurement in heart disease diagnosis and monitoring. *Sensors*, 25(13):4220, July 2025.

[42] Youhe Huang, Hongru Li, Rui Tao, Weiwei Han, Pengfei Zhang, Xia Yu, and Ruikun Wu. A customized framework for coronary artery disease detection using phonocardiogram signals. *Biomedical Signal Processing and Control*, 78:103982, September 2022.

[43] Han Li, Xinpei Wang, Changchun Liu, Peng Li, and Yu Jiao. Integrating multi-domain deep features of electrocardiogram and phonocardiogram for coronary artery disease detection. *Computers in Biology and Medicine*, 138:104914, November 2021.

[44] Yue Rong, Matthew Fynn, Sven Nordholm, Serena Siaw, and Girish Dwivedi. Wearable electro-phonocardiography device for cardiovascular disease monitoring. In *2023 IEEE Statistical Signal Processing Workshop (SSP)*. IEEE, July 2023.

[45] Ingeborg H. Hansen, Karsten Hoppe, Anna Gjerde, Joergen K. Kanters, and Helge B. D. Sorensen. Comparing twelve-lead electrocardiography with close-to-heart patch based electrocardiography. In *2015 37th Annual International Conference of the IEEE Engineering in Medicine and Biology Society (EMBC)*, page 330–333. IEEE, August 2015.

[46] Hong J. Lee, Dong S. Lee, Hyun B. Kwon, Do Y. Kim, and Kwang S. Park. Reconstruction of 12-lead ecg using a single-patch device. *Methods of Information in Medicine*, 56(04):319–327, 2017.

[47] Sofia M. Monteiro and Hugo Plácido da Silva. A novel approach to simultaneous phonocardiography and electrocardiography during auscultation. *IEEE Access*, 11:78224–78236, 2023.

[48] H. S. Cho et al. Development of wireless electronic cardiogram and stethoscope (ecgs) to measure ecg signal and heart sound. *Journal of Biomedical Engineering Research*, 43:124–130, 2022.

[49] Paris B. Lovett, Jason M. Buchwald, Kai Stürmann, and Polly Bijur. The vexatious vital: Neither clinical measurements by nurses nor an electronic monitor provides accurate measurements of respiratory rate in triage. *Annals of Emergency Medicine*, 45(1):68–76, January 2005.

[50] Ian Smith, John Mackay, Nahla Fahrid, and Don Krucheck. Respiratory rate measurement: a comparison of methods. *British Journal of Healthcare Assistants*, 5(1):18–23, January 2011.

[51] Andrew Bates, Martin J. Ling, Janek Mann, and D.K. Arvind. Respiratory rate and flow waveform estimation from tri-axial accelerometer data. In *2010 International Conference on Body Sensor Networks*, page 144–150. IEEE, June 2010.

[52] Sara Lapi, Federico Lavorini, Giovanni Borgioli, Marco Calzolai, Leonardo Masotti, Massimo Pistolesi, and Giovanni A. Fontana. Respiratory rate assessments using a dual-accelerometer device. *Respiratory Physiology amp; Neurobiology*, 191:60–66, January 2014.

[53] Alexander M. Chan, Nima Ferdosi, and Ravi Narasimhan. Ambulatory respiratory rate detection using ecg and a triaxial accelerometer. In *2013 35th Annual International Conference of the IEEE Engineering in Medicine and Biology Society (EMBC)*, page 4058–4061. IEEE, July 2013.

[54] A. R. Fekr, K. Radecka, and Z. Zilic. Tidal volume variability and respiration rate estimation using a wearable accelerometer sensor. In *Proceedings of the 4th International Conference on Wireless Mobile Communication and Healthcare (MobiHealth 2014)*, pages 1–6, Athens, Greece, November 2014. ICST (Institute for Computer Sciences, Social-Informatics and Telecommunications Engineering).

[55] Atena Roshan Fekr, Katarzyna Radecka, and Zeljko Zilic. Design and evaluation of an intelligent remote tidal volume variability monitoring system in e-health applications. *IEEE Journal of Biomedical and Health Informatics*, 19(5):1532–1548, September 2015.

[56] Atena Roshan Fekr, Majid Janidarmian, Katarzyna Radecka, and Zeljko Zilic. Respiration disorders classification with informative features for m-health applications. *IEEE Journal of Biomedical and Health Informatics*, 20(3):733–747, May 2016.

[57] P. D. Hung, S. Bonnet, R. Gillemaud, E. Castelli, and P. T. N. Yen. Estimation of respiratory waveform using an accelerometer. In *Proceedings of the 5th IEEE International Symposium on Biomedical Imaging (ISBI)*, pages 1493–1496, 2008.

[58] Anmin Jin, Bin Yin, G. Morren, H. Duric, and R.M. Aarts. Performance evaluation of a tri-axial accelerometry-based respiration monitoring for ambient assisted living. In *2009 Annual International Conference of the IEEE Engineering in Medicine and Biology Society*, page 5677–5680. IEEE, September 2009.

[59] Guan-Zheng Liu, Yan-Wei Guo, Qing-Song Zhu, Bang-Yu Huang, and Lei Wang. Estimation of respiration rate from three-dimensional acceleration data based on body sensor network. *Telemedicine and e-Health*, 17(9):705–711, November 2011.

[60] Ailton Siqueira, Amanda Franco Spirandeli, Raimes Moraes, and Vicente Zarzoso. Respiratory waveform estimation from multiple accelerometers: An optimal sensor number and placement analysis. *IEEE Journal of Biomedical and Health Informatics*,

23(4):1507–1515, July 2019.

[61] Peter H Charlton, Timothy Bonnici, Lionel Tarassenko, Jordi Alastruey, David A Clifton, Richard Beale, and Peter J Watkinson. Extraction of respiratory signals from the electrocardiogram and photoplethysmogram: technical and physiological determinants. *Physiological Measurement*, 38(5):669–690, April 2017.

[62] Yuyang Miao, Zehua Chen, Chang Li, and Danilo Mandic. Respdiff: An end-to-end multi-scale rnn diffusion model for respiratory waveform estimation from ppg signals, 2024.

[63] Marco A. F. Pimentel, Alistair E. W. Johnson, Peter H. Charlton, Drew Birrenkott, Peter J. Watkinson, Lionel Tarassenko, and David A. Clifton. Toward a robust estimation of respiratory rate from pulse oximeters. *IEEE Transactions on Biomedical Engineering*, 64(8):1914–1923, August 2017.

[64] Priya S. Nandi, Veronica M. Pigott, and David H. Spodick. Sequential cardiac responses during the respiratory cycle: Patterns of change in systolic intervals. *Chest*, 63(3):380–385, March 1973.

[65] Rajkumar Dhar, Seena E. Darwish, Sara A. Darwish, Richard H. Sandler, and Hansen A. Mansy. Effect of respiration and exercise on seismocardiographic signals. *Computers in Biology and Medicine*, 185:109600, February 2025.

[66] Noemi Giordano, Samanta Rosati, Daniele Fortunato, Marco Knaflitz, and Gabriella Balestra. *Personalized Detection of Motion Artifacts for Telemonitoring Applications*. IOS Press, May 2024.

[67] S.P. Preejith, Ahamed Jeelani, Paresh Maniyar, Jayaraj Joseph, and Mohanasankar Sivaprakasam. Accelerometer based system for continuous respiratory rate monitoring. In *2017 IEEE International Symposium on Medical Measurements and Applications (MeMeA)*, page 171–176. IEEE, May 2017.

[68] Yue-Der Lin and Ya-Fen Jhou. Estimation of heart rate and respiratory rate from the seismocardiogram under resting state. *Biomedical Signal Processing and Control*, 57:101779, March 2020.

[69] Stephen Hughes, Haipeng Liu, and Dingchang Zheng. Influences of sensor placement site and subject posture on measurement of respiratory frequency using triaxial accelerometers. *Frontiers in Physiology*, 11, July 2020.

[70] Sankirna D. Joge. Qrs detection using pan–tompkins algorithm from ecg signal, 2021. Retrieved April 22, 2025.

[71] C.L. Mason and L. Tarassenko. Quantitative assessment of respiratory derivation algorithms. In *2001 Conference Proceedings of the 23rd Annual International Conference of the IEEE Engineering in Medicine and Biology Society*, IEMBS-01, page 1998–2001. IEEE.

[72] Noemi Giordano and Marco Knaflitz. A novel method for measuring the timing of heart sound components through digital phonocardiography. *Sensors*, 19(8):1868, April 2019.

[73] D Khodadad, S Nordebo, B Müller, A Waldmann, R Yerworth, T Becher, I Frerichs, L Sophocleous, A van Kaam, M Miedema, N Seifnaraghi, and R Bayford. Optimized breath detection algorithm in electrical impedance tomography. *Physiological Measurement*, 39(9):094001, September 2018.

[74] Marc A. Russo, Danielle M. Santarelli, and Dean O'Rourke. The physiological effects of slow breathing in the healthy human. *Breathe*, 13(4):298–309, November 2017.

[75] Aravind Natarajan, Hao-Wei Su, Conor Heneghan, Leanna Blunt, Corey O'Connor, and Logan Niehaus. Measurement of respiratory rate using wearable devices and applications to covid-19 detection. *npj Digital Medicine*, 4(1), September 2021.